Title

The influence of substrate topography on the migration of corneal epithelial wound borders

Journal

Biomaterials, 34(37)

ISSN

0267-6605

Authors

Yanez-Soto, Bernardo
Liliensiek, Sara J
Gasiorowski, Joshua Z
et al.

Publication Date

2013-12-01

DOI

10.1016/j.biomaterials.2013.08.042

Peer reviewed

Published in final edited form as:
Biomaterials. 2013 December ; 34(37): . doi:10.1016/j.biomaterials.2013.08.042.

The influence of substrate topography on the migration of corneal epithelial wound borders

Bernardo Yanez-Soto[a], **Sara J. Liliensiek**[a], **Joshua Z. Gasiorowski**[b], **Christopher J. Murphy**[c,d], and **Paul F. Nealey**[e,*]

[a]Department of Chemical and Biological Engineering, School of Engineering, University of Wisconsin-Madison, Madison, WI 53706, USA

[b]Department of Biomedical Sciences, Midwestern University, Downers Grove, IL 60515, USA

[c]Department of Veterinary Surgical and Radiological Sciences, School of Veterinary Medicine, University of California Davis, Davis, CA 95616, USA

[d]Department of Ophthalmology and Vision Sciences, School of Medicine, University of California Davis, Davis, CA 95817, USA

[e]Institute for Molecular Engineering, University of Chicago, 5747 South Ellis Avenue, Jones 217, Chicago, IL 60637, USA

Abstract

Currently available artificial corneas can develop post-implant complications including epithelial downgrowth, infection, and stromal melting. The likelihood of developing these disastrous complications could be minimized through improved formation and maintenance of a healthy epithelium covering the implant. We hypothesize that this epithelial formation may be enhanced through the incorporation of native corneal basement membrane biomimetic chemical and physical cues onto the surface of the keratoprosthesis. We fabricated hydrogel substrates molded with topographic features containing specific bio-ligands and developed an *in vitro* wound healing assay. In our experiments, the rate of corneal epithelial wound healing was significantly increased by 50% in hydrogel surfaces containing topographic features, compared to flat surfaces with the same chemical attributes. We determined that this increased healing is not due to enhanced proliferation or increased spreading of the epithelial cells, but to an increased active migration of the epithelial cells. These results show the potential benefit of restructuring and improving the surface of artificial corneas to enhance epithelial coverage and more rapidly restore the formation of a functional epithelium.

Keywords

Biomimetic material; Epithelial cell; Hydrogel; Polyethylene glycol; Nanotopography; Corneal wound healing

1. Introduction

Worldwide, the supply of corneal donor tissue remains insufficient [1], motivating the design, fabrication and use of artificial corneas as a therapy for corneal disorders that cause

*Corresponding author. Tel.: +1 773 702 9143. nealey@uchicago.edu. .
yanezsoto@ucdavis.edu (B. Yanez-Soto)

visual impairment [2]. The artificial corneas currently available focus mainly on the biointegration of the device into the stromal component, with less emphasis on restoring the epithelial layer of the tissue. Inadequate regeneration of a fully functional epithelial covering can lead to problems such as epithelial downgrowth [3], infection [4] and extrusion due to stromal melting [5]. It has been suggested that in order to reduce the aforementioned problems, the ideal artificial cornea should support the normal processes that allow the formation and maintenance of a stratified epithelium over the implant [6]. We hypothesize that the incorporation of biochemical and biophysical cues that have been previously characterized and quantified from the anterior corneal basement membrane [7] will promote epithelial coverage of the implant.

Corneal epithelial wound healing is a highly organized series of events, where the basement membrane has many functions to help maintain a normal stratified epithelium [8–13]. There are several phases during the corneal epithelial wound healing process, including a lag phase (between wounding and initiation of cell migration) where cells alter their metabolic status; a migration phase to cover the bare surface; a proliferation phase and a differentiation phase, where cells stratify and re-establish multiple layers of distinct cells [9,13,14]. In addition to morphological and behavioral alterations, specific signaling components involved in the reformation of the basement membrane (BM) have been reported. Several molecules have been shown to be upregulated in corneal epithelial cells after injury, including fibronectin [15], collagen [16], and laminin-332 (LN332) [17]. These molecules all serve as potential markers to determine whether biophysical and biochemical cues influence the wound healing process.

Previous research from our group, as well as others, has demonstrated that mimicking chemical and physical aspects of the BM of the cornea [7] influenced behaviors essential to the wound healing process in the corneal epithelium, such as adhesion [18], proliferation [19] and migration [20]. These behaviors suggest that topographic cues will have an effect on important phases of the corneal epithelial wound process, translating into an improved rate of wound healing with subsequent stratification and maintenance of a healthy epithelium.

Topographically-molded PEGDA hydrogels functionalized with the adhesive peptide RGD, a sequence found in wounded corneal epithelium BM [21], can provide human corneal epithelial cells (HCECs) with specific biomimetic cues inspired by the BM [22]. Here, we report the use of topographically and biochemically controlled poly(ethylene glycol) diacrylate (PEGDA) hydrogel substrates as an artificial BM simulant to improve the wound healing and functionality of the corneal epithelium.

2. Materials and methods

2.1. Fabrication of biochemically functionalized PEGDA hydrogel substrates with topographic features

Precursor solutions of 20% (w/w) PEGDA were prepared by dissolving PEGDA 3400 in 10 mM 4-(2-hydroxyethyl)-1-piperazineethanesulfonic acid (HEPES) buffer at pH 8.0, with 0.067% (w/v) lithium phenyl-2,4,6-trimethylbenzoylphosphinate (LAP) as the photoinitiator. RGD peptide (Cys–Gly–Gly–Arg–Gly–Asp–Ser–Pro) (UW-Madison Biotechnology Center, WI) was added to the precursor solutions to reach a final concentration of 10 mM. The hydrogel substrates were molded with groove-and-ridge topographic features of different ranges (400 nm, 1400 nm and 4000 nm pitch) or with flat surfaces using a replica-molding technique, as previously reported [22]. Briefly, in a nitrogen atmosphere, a 30 μL drop of the precursor solution was placed on top of a degassed polydimethylsiloxane (PDMS) stamp containing the desired topography with 0.5 mm PDMS

spacers. The precursor solution was then covered by a glass coverslip previously treated with 3-(trichlorosilyl) propyl methacrylate (TPM, Sigma-Aldrich, UK) to ensure adhesion of the gels to the surface. The construct was polymerized under UV-light (364 nm for 900 s at 7.0 mW/cm^2) and the PDMS stamps were peeled off, transferring the pattern to the surface of the hydrogel. Hydrogel substrates were sterilized for 24 h by soaking in 5% isopropyl alcohol (IPA) in 1× phosphate buffered saline (PBS, pH 7.2), rinsed for 24 h in 1× PBS and pre-incubated for 2 h in cell culture media for full equilibration.

2.2. AFM imaging of molded hydrogels

To ensure the incorporation of topographic cues, molded hydrogels containing topographic features were imaged by atomic force microscopy (AFM), using a Nanoscope IIIa Multimode scanning probe microscope (Veeco Instruments Inc., CA). Samples were hydrated in 1× PBS for at least 48 h at room temperature, and scanned in a fluid cell in contact mode using a SNL-10 silicon nitride cantilever with a silicon tip (Veeco Probes, CA).

2.3. HCEC culture

HCECs were harvested from human cadaver corneas graciously provided by the Lions Eye Bank of Wisconsin, Madison or the Missouri Lions Eye Bank (Columbia, MO) as previously reported [23]. Cells from two to four corneas were centrifuged and re-suspended in epithelial medium (EP medium). EP medium is composed of a 3:2 ratio of Ham's F12:Dulbecco's Modified Eagle medium (DMEM) (Invitrogen, CA), supplemented with 2.5% (v/v) fetal bovine serum (FBS), 0.4 μg/mL hydrocortisone, 8.4 ng/mL cholera toxin, 5 μg/mL insulin, 24 μg/mL adenine, 10 ng/mL epidermal growth factor, 100 units penicillin and 100 μg/mL streptomycin [24]. All HCECs were incubated on plates seeded with a feeder layer of Swiss mouse 3T3 fibroblasts previously treated with 4 μg/mL of mitomycin-C for 2 h. HCECs were incubated at 37 °C and 5% CO_2 until they reached approximately 70% confluence. HCECs were used between passages 1 and 4.

2.4. Wound healing assay

HCECs at 60–70% confluence were exposed to 0.01% EDTA in 1× PBS for 1 min to allow detachment of feeder cells. For live fluorescence staining, cells were incubated with a 6 μM live dye solution of CellTracker green CMFDA (5-Chloromethyl fluorescein diacetate, Life Technologies, NY) in DMEM for 45 min at 37 °C and 5% CO_2 as recommended by the manufacturer. The dye solution was then replaced with fresh EP medium, and cells were incubated for another 45 min at 37 °C and 5% CO_2. After live staining, cells were harvested using 0.025% Trypsin/0.01% EDTA, centrifuged and re-suspended in EP medium, and plated at a density of 150,000 cells/cm^2 on hydrogel surfaces around a 5 mm diameter cloning cylinder to act as an 'exclusion zone' (Fig. 1). After incubation for 24 h, the cloning cylinders were removed and the fluorescently labeled cells on the hydrogel samples were imaged at 0 h, 24 h, 48 h and 72 h using a Stemi SV11 dissecting microscope (Zeiss, NY) with a 1.2× objective lens. The area of the wound was measured using AxioVision software version 4.8 (Zeiss, NY). The size of the wound was defined as the radius (R) of the circle of the measured area (A), using the equation $R = (A/\pi)^{1/2}$, and the wound closure was defined as the difference of the radius from the radius of the starting point ($\Delta R = R_O - R$). From the wound closure data, a linear regression was performed, and the slope was reported as the wound healing rate in mm/hour. An experimental set consisted of at least four replicates of each hydrogel substrate. Each experimental set was repeated in triplicate.

2.5. Proliferation assay

The assessment of cell proliferation was measured through the incorporation of 5-ethynyl-2′-deoxyuridine (EdU) with the Click-iT EdU Cell Proliferation Assay Kit (Invitrogen, CA). HCECs were plated using the wound healing method described above. For the starting time point, cells were incubated in 10 μM EdU for 12 h before removal of the cloning cylinders. For subsequent time points (12 h, 24 h and 36 h), the cloning cylinders were removed and HCECs were incubated for 12 h in 10 μM EdU prior to the corresponding time point. At each corresponding time point, cells were fixed and permeabilized and the EdU was stained according to the manufacturer's protocol. The nuclei of cells that replicated in the 12 h period of incubation with EdU were labeled in red. Cells were also stained with 0.1 μg/mL 4′,6-Diamidino-2-phenylindole (DAPI) (Invitrogen, CA) in 1× PBS for 30 min, which permitted the detection of all nuclei (blue).

Fluorescence microscopy was used to quantify the percentage of cells that incorporated EdU in the 12-hour incubation period with respect to the total number of cells. The area of the confluent layer was measured, and the cell density was reported as the total number of cells/area. At least three images were analyzed for each topography in each experiment, and the experiments were repeated in triplicate.

2.6. Immunocytochemistry and analysis of LN332 expression and location

For the purpose of evaluating the migratory status of cells upon epithelial wounding, we analyzed the expression and location of LN332 (also designated as laminin-5) in HCECs. Following each time point, cells were fixed with a 1% paraformaldehyde solution in 1× PBS at room temperature for 20 min. Cells were then permeabilized with 0.1% (w/v) Triton X-100 (Sigma–Aldrich, St Louis, MO) in 1× PBS for 7 min, followed by exposure to a solution of 1% (w/v) bovine serum albumin (Sigma–Aldrich, St Louis, MO) and 1% goat serum (Sigma–Aldrich, St Louis, MO) in 1× PBS for 20 min to block non-specific binding. Cells were then incubated with 5 μg/mL of mouse anti-laminin-5 IgG clone P3H9-2 (Millipore, MA) for 1 h, rinsed in 1× PBS and incubated in 2 μg/mL of AlexaFluor 488 labeled goat anti-mouse IgG (Invitrogen, CA) for 1 h to label laminin-5 (green). Cells were rinsed with 1× PBS and incubated in 0.1 μg/mL DAPI in 1× PBS for 30 min, to label the nucleus (blue). To demonstrate the specificity of the staining, experiments with secondary antibody alone served as the negative control. Images of fluorescently stained cells on the corneal epithelial edge of the wound were obtained for each substrate using a 10× objective lens. On each topographic substrate at least four images were taken. Image analysis was performed using AxioVision software (Zeiss, NY). The border of the wound was defined as the area 50 μm peripheral to the migrating front of the wound edge. The fluorescence density of that area was measured and divided by the number of cells in that area. This was normalized to the fluorescence level per cell of the flat surface at the starting time point to obtain the relative expression of laminin-5 per cell in the wound border. At least three substrates for each topography were analyzed for each experiment, and experiments were repeated in triplicate.

2.7. Statistics

Experimental data were analyzed using analysis of variance (ANOVA). When variability was determined to be significant ($\alpha = 0.05$) the Bonferroni multiple comparison test was used to determine significance between flat surfaces and topographic surfaces. Significant results were further divided into "statistically significant" ($0.01 \leq p \leq 0.05$, *), "very significant" ($0.001 \leq p < 0.01$, **), and "extremely significant" ($p < 0.001$, ***).

3. Results

3.1. Molding of topographic features

To ensure the incorporation of topographic cues onto the substrates, PEG hydrogels functionalized with RGD peptide were fabricated by soft lithography using nano- and micro-patterned PDMS molds. The precursor solution consisted of a mixture of PEGDA previously reacted with a cysteine-ended peptide and photoinitiator. The hydrogels were synthesized with the presence of a UV source, creating a crosslinked network that retained the anisotropic ridge and groove pattern of the stamp, as exhibited by the AFM images in Fig. 2. The pitches used in our experiments were 400 nm, 1400 nm and 4000 nm, and the depth of the grooves ranged from 200 to 400 nm.

3.2. Influence of topography in wound healing in vitro

Fluorescently stained HCECs were cultured to confluence on hydrogel substrates functionalized with RGD peptide, using a 5 mm diameter cloning cylinder as an “exclusion zone”. 24 h after reaching confluency, the cylinder was removed; creating a circular wound that was imaged at 0 h, 24 h, 48 h, 72 h and 96 h. The area of each wound at every time point was measured, and the wound advance rate was quantified as described above. The closure of the wounds is demonstrated in Fig. 3, where we observed increased wound closure at earlier time points on the topographic surfaces, compared to the flat surfaces. Compared to chemically identical flat surfaces, hydrogel substrates molded with topography (400 nm, 1400 nm and 4000 nm pitch) demonstrated significant increases in the wound advance. This was observed at 24 h after removal of the restricting cloning chamber, and persisted up through 96 h after removal (Fig. 4A). The wound healing rate on all the topographically patterned substrates was significantly increased compared to the flat substrates ($p < 0.001$), with 52%, 62% and 43% faster rates on the 400 nm, 1400 nm and 4000 nm pitch substrates respectively (Fig. 4B). In our studies we found that single cells usually exhibit contact guidance in response to the topographic features. Interestingly, the wound border of the confluent epithelial sheet did not appear to have an asymmetric closure indicative of contact guidance (i.e. the wound area did not assume an orientation parallel to the substrate grooves as healing progressed). Based on this observation, we analyzed the cell alignment on the border of the wound at higher magnification with an inverted phase microscope (10× objective, Fig. 5). On topographically patterned substrates, isolated cells away from the wound border aligned their long axis parallel to the long axis of the underlying topography, but cells contained within the border of the wound did not exhibit any such alignment.

3.3. Proliferation and spreading on flat and topographically patterned substrates

Proliferation assays were performed on *in vitro* wounds by observing the incorporation of EdU into the DNA of replicating cells. After incubation in EdU for 12 h, cells were fixed, EdU was labeled in red to identify proliferating cells and the cell nuclei were stained using DAPI (blue). The wound edges were then imaged with an inverted fluorescence microscope. Representative images are shown in Fig. 6A, where no qualitative differences between cells on topography vs. planar surfaces were observed. To verify, proliferating cells as well as non-proliferating cells were counted and the percentage of proliferating cells was calculated at 0 h, 12 h, 24 h and 36 h for all substrates. Fig. 6B shows the quantitative results. While a significant difference in proliferation between different time points was observed, there was no difference as a result of topographic patterning. Cell density was also calculated by dividing the total number of cells on the surface by the area they covered. Again, as depicted in Fig. 6C, we observed significant differences in cell density between the time points but no difference as a result of topographic patterning. Upon closer examination of the images shown in Fig. 6A, we noted that the cells adjacent to the edge of the wound were not

proliferating and their nuclei appeared to be larger. This observation motivated further investigation regarding the expression of LN332 as a biomarker for cell migration in response to topographic cues.

3.4. Expression of LN332 on the border of wounds on flat and topographically patterned substrates

HCECs were once again plated for experiments as described above, fixed at 0 h, 12 h, 24 h and 48 h after wounding, and immunolabeled with antibodies directed against LN332. Images of the wound border were obtained via fluorescence microscopy. Representative images of the wound border are shown in Fig. 7. An increased expression of LN332 can be observed for the 48 h time point on all topographic substrates. Tracks displaying the spatial expression patterns of LN332 within the migration path were also observed. The total LN332 fluorescence of the area 50 μm next to the wound edge was quantified, along with the total number of cells in that area. Fig. 8 shows the relative fluorescence per cell in the wound border. Compared to the flat surfaces, a very significant increase in the relative expression of LN332 per cell on the wound edge of topographic substrates can be clearly observed after 12 h (66% for 400 nm, 83% for 1400 nm and 71% for 4000 nm); and after 24 h (142% for 400 nm, 129% for 1400 nm and 147% for 4000 nm). The relative amount of LN332 expression per cell on the flat substrates appears to remain constant throughout the experiment.

4. Discussion

The healing and regeneration of the corneal epithelium is a complex and ordered process highly dependent on a balance of cell behaviors, such as adhesion [18], proliferation [19], differentiation [14], migration [20] and cell death [13]. Those behaviors are regulated by the simultaneous integration of signals that originate from the cellular microenvironment including cell–cell communication, soluble molecules, and interactions with the biophysical and chemical attributes of the ECM [25–28]. Our group has demonstrated that the topographic cues intrinsic to the native BM [7], unequivocally influence wound healing behaviors [18–20]. Parkinson et al. demonstrated that the size of nano-pores on aluminum oxide membranes influenced the rate of keratocyte proliferation and migration *in vitro* [29]. In addition, the use of topographically patterned membranes as dressings lead to less granulation tissue and a more mature epidermal layer in skin than control standard burn dressings *in vivo* [30].

The results of the studies reported above provide additional evidence that the provision of substratum topographic cues effectively improves corneal epidermal wound closure. Although we anticipated a preferred directionality of the migration of the wound border parallel to the long axis of the underlying topographic features, the wound closure trajectory was mostly uniform. Previous research on topographic cues and cell migration conducted by our laboratory showed that single human corneal epithelial cells plated on SiO_2 topographic substrates migrated preferentially parallel to the long axis of the topographic features [20]. Colonies of cells also presented a preferential dispersion along the topographic features, although this effect was small, and migration perpendicular to the topography was always present [20]. Recent unpublished work from our laboratory conducted on PEGDA hydrogels also demonstrates less contact guided migration in epithelial confluent sheets compared to single cell studies (Wilson, M.J., personal communication). These results suggest that, upon wounding, epithelial cells in a confluent sheet respond to the presence of topographic cues, but do not exhibit the same degree of contact guided migration evidenced by single cells.

To elucidate the mechanisms leading to the increased wound closure when cells are in contact with topography, we investigated possible changes in proliferation, cell spreading

and migration. The uniform cell-spreading observed on all the surfaces is consistent with other published results employing similar substrates and media as used in this report [22]. However, the lack of an effect of topographic cues in modulating cell proliferation was an unexpected result. We have previously reported that the proliferation of an immortalized cell line (SV40-HCECs), as well as primary cells, decreased when seeded onto small scale topographic features characteristic of native basement membranes [19]. The proliferation decrease seen in isolated cells seeded on topography, though, was not observed in the confluent epithelial sheets investigated in this manuscript.

Additionally, to determine if cells in the border of the wound are actively migrating, or simply being displaced by the proliferating cells behind, we investigated the localized expression of LN332. LN332 is a major component in the corneal BM [8] and its increased expression has been correlated with migration [31]. A dual function of LN332 has been proposed where LN332 can act both as a promoter for cell adhesion or migration, depending on the processing stage of the molecule [8]. Human LN332 is initially synthesized as a protein containing a 190 kDa α3 chain, a 135 kDa β3 chain and a 150 kDa γ2 chain [32]. The molecule increases its adhesive activity upon cleavage of the α3 subunit into a 160 kDa isoform [33]. This mature form of LN332 supports the formation of hemidesmosomes, linking the ECM with the keratin cytoskeleton via the integrin α6β4 [34–36]. The mature LN332 can also support the formation of focal adhesions by binding to the integrin α3β1, which links the ECM to the actin cytoskeleton [37]. The deposition of LN332 occurs on the posterior edge of cells, in a trail that follows the path of migration [38]. During epidermal wound healing the γ2 subunit is cleaved into a 105 kDa isoform, which increases cell motility and decreases cell adhesion [39]. The isoform containing the cleaved γ2 subunit is unable to assemble in the ECM [40] and this molecule works as a motility-inducing soluble factor [41]. It has been suggested that this motility is triggered by the binding of the cleaved γ2 subunit to the epidermal growth factor receptor (EGFR) [42]. Although the mechanism is not completely understood, it is believed that bone morphogenetic protein 1 (BMP-1) and mammalian tolloid metalloproteinase (mTLD) are responsible for the processing of the γ2 chain [43,44].

The observed LN332 expression is consistent with a model originally proposed for the regulation of tumor cell migration [32]: HCECs on topographically patterned substrates express and postprocess the γ2-cleaved form of LN332 on the wound border, enhancing the rate of migration of the cells and orienting the cells to move towards the center of the wound. This hypothesis is consistent with research performed by our laboratory, demonstrating that the broad expression of ECM proteins is down-regulated on topographic substrates compared to planar controls [45].

In summary, we fabricated substrates with biomimetic topographic features that enhanced the closure of epithelial wounds *in vitro*. These attributes can be incorporated into keratoprosthetics that our data suggest would promote epithelialization and improve clinical outcomes. Future studies will further explore the role of important BM components, such as LN332, and the incorporation of our hydrogel platform onto artificial corneas for *in vivo* experiments using animal models.

5. Conclusions

Substrates made with PEGDA hydrogels functionalized with molecules that induce specific interactions with primary HCECs showed improved rates of healing when topographic features were present. We determined that the enhanced rate of wound closure is due to increased active migration of the wound border towards the center of the simulated injured area. In addition, we elucidated some possible mechanisms of the cellular response upon

wounding in the presence of topography involving the expression and processing of BM molecules. Finally, our data suggest that biophysical cues alter the spatial expression of LN332, which may be a possible signaling mechanism that ultimately produces the wound healing results seen on topographically patterned surfaces. This study demonstrates that topographic cues are a fundamental parameter of native extracellular matrices and consideration should be given for including these ubiquitous and potent attributes in the engineering of biomimetic materials.

Acknowledgments

This work is supported in part by NIH-National Eye Institute (1RO1EY017367-01A and 1RO1EY016134-01A2), and by the American Recovery and Reinvestment Act of 2009 through the NIH-National Institute of Arthritis and Musculoskeletal and Skin Diseases (5RC2AR058971-01), and its contents are solely the responsibility of the authors and do not necessarily represent the official views of the National Eye Institute, the National Institute of Arthritis and Musculoskeletal and Skin Diseases or the NIH. The authors wish to thank Ana Kiyanova for providing molds and Dr. Michelle Wilson for providing the photoinitiator and technical support.

References

[1]. Aiken-O'Neill P, Mannis MJ. Summary of corneal transplant activity – Eye Bank Association of America. Cornea. 2002; 21:1–3. [PubMed: 11805497]

[2]. Whitcher JP, Srinivasan M, Upadhyay MP. Corneal blindness: a global perspective. Bull World Health Organ. 2001; 79:214–21. [PubMed: 11285665]

[3]. Aldave AJ, Kamal KM, Vo RC, Yu F. The Boston type I keratoprosthesis: improving outcomes and expanding indications. Ophthalmology. 2009; 116:640–51. [PubMed: 19243830]

[4]. Barnes SD, Dohlman CH, Durand ML. Fungal colonization and infection in Boston keratoprosthesis. Cornea. 2007; 26:9–15. [PubMed: 17198007]

[5]. Jiraskova N, Rozsival P, Burova M, Kalfertova M. AlphaCor artificial cornea: clinical outcome. Eye (London). 2011; 25:1138–46.

[6]. Hicks CR, Fitton JH, Chirila TV, Crawford GJ, Constable IJ. Keratoprostheses: advancing toward a true artificial cornea. Surv Ophthalmol. 1997; 42:175–89. [PubMed: 9381372]

[7]. Abrams GA, Schaus SS, Goodman SL, Nealey PF, Murphy CJ. Nanoscale topography of the corneal epithelial basement membrane and Descemet's membrane of the human. Cornea. 2000; 19:57–64. [PubMed: 10632010]

[8]. Ebihara N, Mizushima H, Miyazaki K, Watanabe Y, Ikawa S, Nakayasu K, et al. The functions of exogenous and endogenous laminin-5 on corneal epithelial cells. Exp Eye Res. 2000; 71:69–79. [PubMed: 10880277]

[9]. Bentley E, Murphy CJ. Topical therapeutic agents that modulate corneal wound healing. Vet Clin North Am Small Anim Pract. 2004; 34:623. [PubMed: 15110975]

[10]. Germain L, Carrier P, Auger FA, Salesse C, Guerin SL. Can we produce a human corneal equivalent by tissue engineering? Prog Retin Eye Res. 2000; 19:497–527. [PubMed: 10925241]

[11]. Myung D, Duhamel PE, Cochran JR, Noolandi J, Ta CN, Frank CW. Development of hydrogel-based keratoprostheses: a materials perspective. Biotechnol Prog. 2008; 24:735–41. [PubMed: 18422366]

[12]. Reid B, Song B, McCaig CD, Zhao M. Wound healing in rat cornea: the role of electric currents. FASEB J Off Publ Fed Am Soc Exp Biol. 2005; 19:379–86.

[13]. Lu L, Reinach PS, Kao WW. Corneal epithelial wound healing. Exp Biol Med (Maywood). 2001; 226:653–64. [PubMed: 11444101]

[14]. Dalton BA, Evans MD, McFarland GA, Steele JG. Modulation of corneal epithelial stratification by polymer surface topography. J Biomed Mater Res. 1999; 45:384–94. [PubMed: 10321712]

[15]. Nishida T, Awata T, Ohashi Y, Suda T, Inoue Y, Manabe R, et al. Dynamics of fibronectin in corneal wound healing: immunohistochemical study of experimental bullous keratopathy in rabbits. Cornea. 1982; 1:311.

[16]. Gipson IK, Spurr-Michaud SJ, Tisdale AS. Hemidesmosomes and anchoring fibril collagen appear synchronously during development and wound healing. Dev Biol. 1988; 126:253–62. [PubMed: 3350210]

[17]. Nguyen BP, Ryan MC, Gil SG, Carter WG. Deposition of laminin 5 in epidermal wounds regulates integrin signaling and adhesion. Curr Opin Cell Biol. 2000; 12:554–62. [PubMed: 10978889]

[18]. Karuri NW, Liliensiek S, Teixeira AI, Abrams G, Campbell S, Nealey PF, et al. Biological length scale topography enhances cell-substratum adhesion of human corneal epithelial cells. J Cell Sci. 2004; 117:3153–64. [PubMed: 15226393]

[19]. Liliensiek SJ, Campbell S, Nealey PF, Murphy CJ. The scale of substratum topographic features modulates proliferation of corneal epithelial cells and corneal fibroblasts. J Biomed Mater Res Part A. 2006; 79:185–92.

[20]. Diehl KA, Foley JD, Nealey PF, Murphy CJ. Nanoscale topography modulates corneal epithelial cell migration. J Biomed Mater Res Part A. 2005; 75:603–11.

[21]. Tuori A, Uusitalo H, Burgeson RE, Terttunen J, Virtanen I. The immunohisto-chemical composition of the human corneal basement membrane. Cornea. 1996; 15:286–94. [PubMed: 8713932]

[22]. Yanez-Soto B, Liliensiek SJ, Murphy CJ, Nealey PF. Biochemically and topo-graphically engineered poly(ethylene glycol) diacrylate hydrogels with biomimetic characteristics as substrates for human corneal epithelial cells. J Biomed Mater Res Part A. 2013; 101A:1184–94.

[23]. Teixeira AI, Abrams GA, Bertics PJ, Murphy CJ, Nealey PF. Epithelial contact guidance on well-defined micro- and nanostructured substrates. J Cell Sci. 2003; 116:1881–92. [PubMed: 12692189]

[24]. Allen-Hoffmann BL, Rheinwald JG. Polycyclic aromatic hydrocarbon muta-genesis of human epidermal keratinocytes in culture. Proc Natl Acad Sci U S A. 1984; 81:7802–6. [PubMed: 6440145]

[25]. Place ES, Evans ND, Stevens MM. Complexity in biomaterials for tissue engineering. Nat Mater. 2009; 8:457–70. [PubMed: 19458646]

[26]. Lutolf MP, Hubbell JA. Synthetic biomaterials as instructive extracellular microenvironments for morphogenesis in tissue engineering. Nat Biotechnol. 2005; 23:47–55. [PubMed: 15637621]

[27]. Stevens MM, George JH. Exploring and engineering the cell surface interface. Science. 2005; 310:1135–8. [PubMed: 16293749]

[28]. Mitragotri S, Lahann J. Physical approaches to biomaterial design. Nat Mater. 2009; 8:15–23. [PubMed: 19096389]

[29]. Parkinson LG, Giles NL, Adcroft KF, Fear MW, Wood FM, Poinern GE. The potential of nanoporous anodic aluminium oxide membranes to influence skin wound repair. Tissue Eng Part A. 2009; 15:3753–63. [PubMed: 19527180]

[30]. Parkinson LG, Rea SM, Stevenson AW, Wood FM, Fear MW. The effect of nanoscale topography on keratinocyte phenotype and wound healing following burn injury. Tissue Eng Part A. 2012; 18:703–14. [PubMed: 21988618]

[31]. Daniels JT, Geerling G, Alexander RA, Murphy G, Khaw PT, Saarialho-Kere U. Temporal and spatial expression of matrix metalloproteinases during wound healing of human corneal tissue. Exp Eye Res. 2003; 77:653–64. [PubMed: 14609553]

[32]. Miyazaki K. Laminin-5 (laminin-332): unique biological activity and role in tumor growth and invasion. Cancer Sci. 2006; 97:91–8. [PubMed: 16441418]

[33]. Tsubota Y, Yasuda C, Kariya Y, Ogawa T, Hirosaki T, Mizushima H, et al. Regulation of biological activity and matrix assembly of laminin-5 by COOH-terminal, LG4-5 domain of alpha 3 chain. J Biol Chem. 2005; 280:14370–7. [PubMed: 15695818]

[34]. Hamill KJ, Paller AS, Jones JCR. Adhesion and migration, the diverse functions of the laminin alpha 3 subunit. Dermatol Clin. 2010; 28:79. [PubMed: 19945619]

[35]. Mercurio AM, Rabinovitz I, Shaw LM. The α6β4 integrin and epithelial cell migration. Curr Opin Cell Biol. 2001; 13:541–5. [PubMed: 11544021]

[36]. Goldfinger LE, Stack MS, Jones JC. Processing of laminin-5 and its functional consequences: role of plasmin and tissue-type plasminogen activator. J Cell Biol. 1998; 141:255–65. [PubMed: 9531563]

[37]. Margadant C, Raymond K, Kreft M, Sachs N, Janssen H, Sonnenberg A. Integrin α3β1 inhibits directional migration and wound re-epithelialization in the skin. J Cell Sci. 2009; 122:278–88. [PubMed: 19118220]

[38]. Frank DE, Carter WG. Laminin 5 deposition regulates keratinocyte polarization and persistent migration. J Cell Sci. 2004; 117:1351–63. [PubMed: 14996912]

[39]. Ogawa T, Tsubota Y, Maeda M, Kariya Y, Miyazaki K. Regulation of biological activity of laminin-5 by proteolytic processing of gamma 2 chain. J Cell Biochem. 2004; 92:701–14. [PubMed: 15211568]

[40]. Gagnoux-Palacios L, Allegra M, Spirito F, Pommeret O, Romero C, Ortonne J, et al. The short arm of the laminin γ2 chain plays a pivotal role in the incorporation of laminin 5 into the extracellular matrix and in cell adhesion. J Cell Biol. 2001; 153:835–50. [PubMed: 11352943]

[41]. Kariya Y, Miyazaki K. The basement membrane protein laminin-5 acts as a soluble cell motility factor. Exp Cell Res. 2004; 297:508–20. [PubMed: 15212952]

[42]. Schenk S, Hintermann E, Bilban M, Koshikawa N, Hojilla C, Khokha R, et al. Binding to EGF receptor of a laminin-5 EGF-like fragment liberated during MMP-dependent mammary gland involution. J Cell Biol. 2003; 161:197–209. [PubMed: 12695504]

[43]. Amano S, Scott IC, Takahara K, Koch M, Champliaud MF, Gerecke DR, et al. Bone morphogenetic protein 1 is an extracellular processing enzyme of the laminin 5 γ2 chain. J Biol Chem. 2000; 275:22728–35. [PubMed: 10806203]

[44]. Veitch DP, Nokelainen P, McGowan KA, Nguyen TT, Nguyen NE, Stephenson R, et al. Mammalian tolloid metalloproteinase, and not matrix metalloprotease 2 or membrane type 1 metalloprotease, processes laminin-5 in keratinocytes and skin. J Biol Chem. 2003; 278:15661–8. [PubMed: 12473650]

[45]. Gasiorowski JZ, Liliensiek SJ, Russell P, Stephan DA, Nealey PF, Murphy CJ. Alterations in gene expression of human vascular endothelial cells associated with nanotopographic cues. Biomaterials. 2010; 31:8882–8. [PubMed: 20832112]

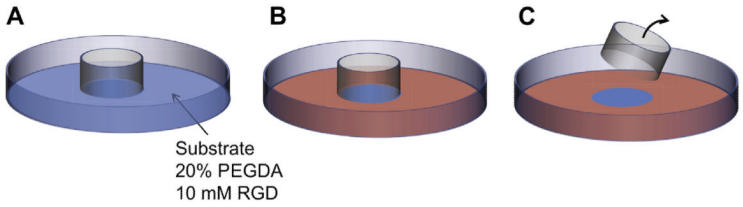

Fig. 1.

Wound healing assay for the testing of topographic substrates. A) The bottom of a culture dish is covered with the PEGDA substrates patterned with topographic ridges and grooves. A cloning cylinder is placed on top to act as an exclusion zone. B) HCECs are cultured on the substrates, until confluent. C) The cloning cylinder is removed, creating a simulated wound.

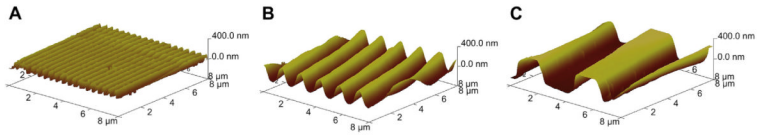

Fig. 2.
AFM images of equilibrium-hydrated hydrogels, showing the molding of the topographic features of A) 400 nm, B) 1400 nm and C) 4000 nm pitch.

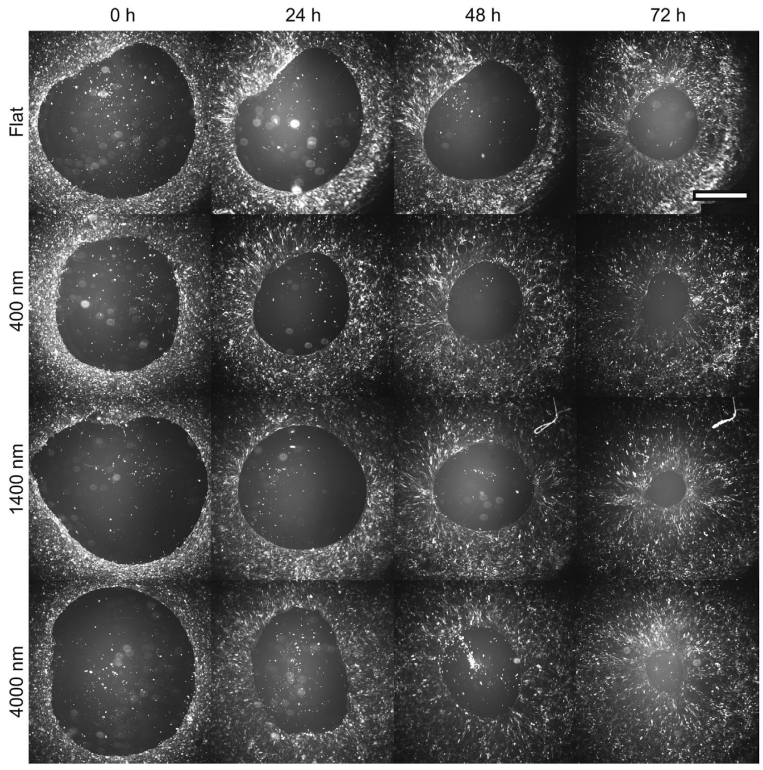

Fig. 3.

Closure of the wounds on control flat surfaces, and on topographies of 400 nm, 1400 nm and 4000 nm pitch after 24 h, 48 h and 72 h. Increased wound closures can be appreciated on topographic substrates. The direction of the topographic features (grooves and ridges) is vertical. The closure of the wounds does not appear to be contact guided. Scale bar: 2 mm.

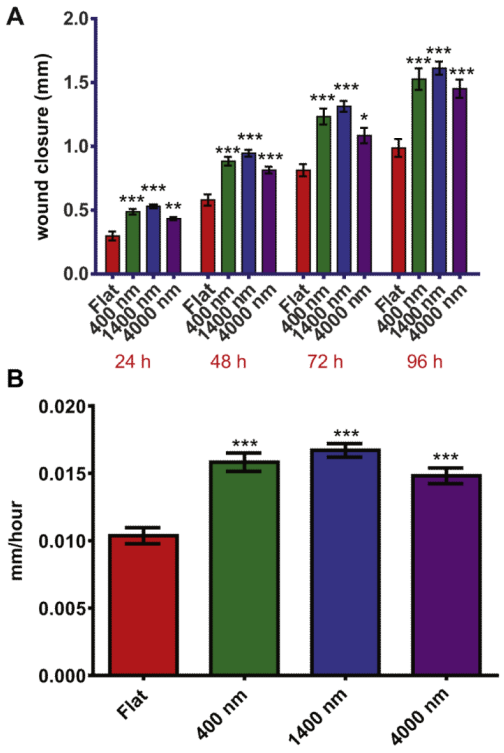

Fig. 4.

The wound closure is increased on topographic substrates, compared to planar surfaces. A) The wound border advanced on topography faster than on flat surfaces, starting 24 h after wounding. B) The wound closure rate is approximately 50% faster on topographic substrates. Error bars: SEM (***$p \leq 0.001$; **$0.001 < p \leq 0.01$; *$0.01 < p \leq 0.05$).

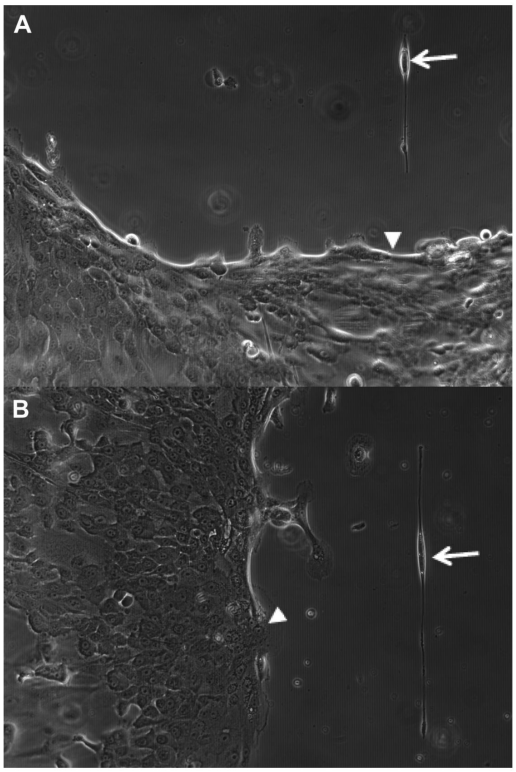

Fig. 5.
Close up phase microscopy images (10×) of the wound border on 4000 nm pitch, 48 h after wounding. On single cells detached from the wound, elongation and alignment of the cells can be observed (arrows). No contact guidance was exhibited by cells on the border of the wound (arrowheads). A) Wound border perpendicular to topography. B) Wound border parallel to topography.

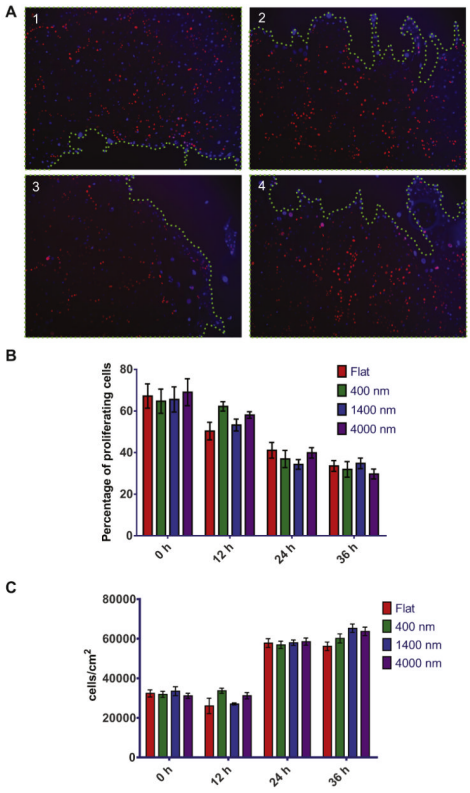

Fig. 6.

EdU proliferation assay. A) Images of the wound border on the different substrates. Cells proliferating are stained in red. Cell nuclei were counter stained in blue (DAPI). B) The percentage of proliferating cells at each time point is not significantly different for any of the substrates used. Proliferation is uniformly reduced after 36 h. C) Cell density is not significantly different at each time point for our substrates. Error bars: SEM.

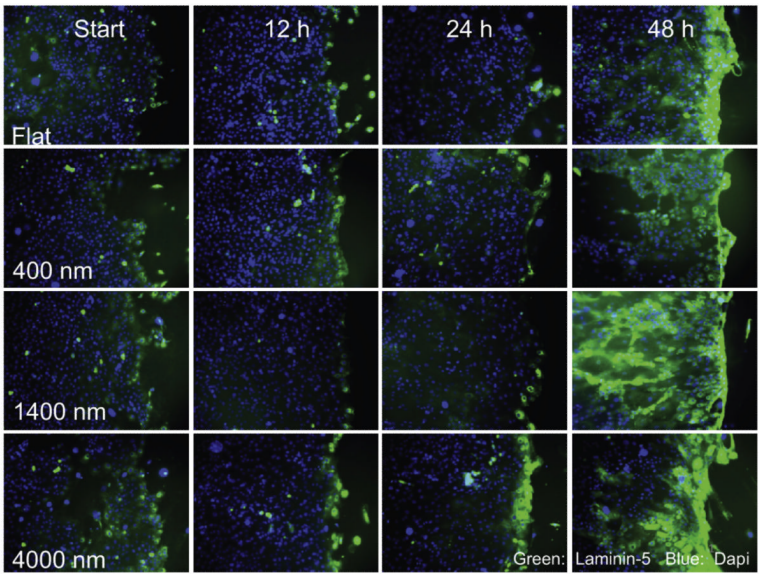

Fig. 7.

Images of the wound border at 0 h, 12 h and 48 h with LN332 stained in green. Cell nuclei are stained in blue. The increase in expression on the border of the wound is apparent for the topographic features after 48 h. Deposition of LN332 following the cellular track of migration can be clearly observed for 1400 nm at the 48 h time point.

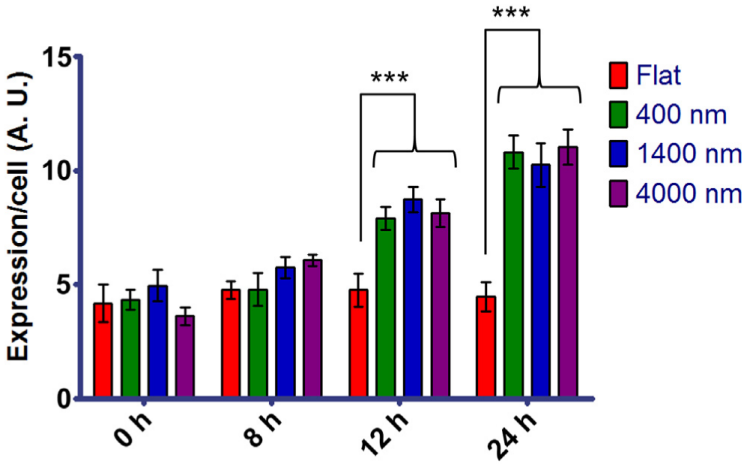

Fig. 8.

Relative quantified immunofluorescence expression per cell of LN332 on the wound border. After 12 h, cells on the wound border on topographic features presented a 1.5-fold increased expression vs. cells on flat surfaces. After 24 h, the increased expression on topography was 2-fold. Error bars: SEM (***$p \leq 0.001$).